JOURNAL OF CATALYSIS 138, 70–78 (1992)

Kinetics of CO Oxidation by N_2O over Rh(111)

DAVID N. BELTON AND STEVEN J. SCHMIEG

Physical Chemistry Department, General Motors Research Laboratories, Warren, Michigan 48090

Received March 24, 1992; revised June 19, 1992

We have studied, for the first time, the reaction of CO with N_2O over a Rh(111) catalyst at pressures between 1 and 20 Torr in an apparatus that couples a moderate pressure reactor with an ultrahigh vacuum analysis chamber. Using 4 Torr of CO and 4 Torr of N_2O between 570 and 670 K, we measured an apparent activation energy (E_a) of 40.0 kcal/mol. By varying the reactant pressures (T = 623 K), we determined that the reaction orders are +1.1 in N_2O pressure and −1.2 in CO pressure. Both E_a and the reaction order are in good agreement with previously reported measurements over alumina supported Rh particles. Kinetic modeling of the data suggests that CO and N_2O compete for a limited number of vacant sites on a surface where $\Theta_{CO} \geq 0.9$ ML. Under these conditions, the rate limiting step is N_2O dissociation. We estimate, based on the model, that the barrier for N_2O dissociation ($E_{diss}^{N_2O}$) is 17.5 kcal/mol. The model also predicts that the N_2O sticking coefficient (S_{N_2O}) must be greater than 0.005. Our measurements show that there is excellent agreement between Rh(111) and supported Rh reaction kinetics with regards to both E_a and the CO pressure dependence. These experimental results add still another reaction to the growing list of cases where single crystals are excellent models for more practical supported catalysts. Further, our modeling of these results allows us to estimate two previously unknown quantities, S_{N_2O} and $E_{diss}^{N_2O}$.

1. INTRODUCTION

Rh is included in current automotive catalytic converters in large part because of its superior activity for the reduction of nitrogen oxides to nitrogen (*1, 2*).

In fact, the automotive industry is by far the largest consumer of Rh metal, the demand for which continues to increase as more stringent emission control standards are implemented worldwide. As a part of our effort to take maximum advantage of Rh's unique activity as an automotive exhaust catalyst, we have studied the kinetics for the CO + N_2O reaction over a Rh(111) single crystal at partial pressures comparable to those present in automotive exhaust systems. N_2O can form over Rh catalysts as a result of the partial reduction of NO by CO (*3–10*) or hydrocarbons. N_2O emissions are undesirable for two reasons: N_2O emissions are regulated under current NO_x emission standards which will soon be even lower and N_2O is an important "greenhouse gas." Both of these facts point out how important it is that N_2O formation in the catalytic converter be avoided. It has been proposed (*3, 4*) that N_2O formed by the reaction of CO and NO can be subsequently removed by further reaction with CO:

$$CO + N_2O \rightarrow N_2 + CO_2.$$

When this reaction is run over a single-crystal model catalyst, we obtain the specific rate and product distributions with a high degree of certainty. By coupling these measurements with the wealth of single-crystal data that exists for the elementary reaction steps, we can obtain a more detailed understanding of the reaction kinetics than is possible for conventional supported catalyst. In cases where the reactivity of the single crystal is the same as that of conventional catalysts (*11–13*), we gain new insight into the workings of practical catalysts.

For Rh/Al_2O_3 catalysts of the type which are important for automotive applications, N_2O is the major product of the CO + NO

0021-9517/92 $5.00

reaction at low temperatures and conversion; but, only N_2 is observed at very high temperatures and 100% conversion (*3, 4, 6*). One explanation of the observed selectivity is that N_2O is reduced at the higher temperatures and conversions by reaction with CO (*3, 4*). Recently we reexamined the CO + NO reaction over Rh(111) and found that N_2O is a major reaction product (*14*) for the single-crystal catalyst, just as for supported Rh. This observation led to the present study of the CO + N_2O reaction. To our knowledge, the CO + N_2O reaction has not been studied over Rh single crystals and thus warrants attention. Interestingly, we observe essentially the same reaction kinetics and reaction orders as were reported by McCabe and Wong (*4*) for alumina-supported Rh. Our data are fit very well with a kinetic model based on the mechanism proposed by McCabe and Wong (*4*). This modeling suggests that the dissociation of adsorbed N_2O is the rate-limiting step (RLS) of the reaction which is occurring on a surface which has a very high ($\geq$0.9 ML) CO coverage.

2. EXPERIMENTAL ASPECTS

2.1. Apparatus and Procedures

The experiments were performed in a custom-built system which couples an ultrahigh vacuum (UHV) analysis chamber with a moderate-pressure ($\leq$100 Torr) reactor. The reactor and analysis chambers are separated with a gate-valve. The UHV analysis chamber is equipped with a wide array of analytical techniques. For this study we used low-energy electron diffraction (LEED), X-ray photoelectron spectroscopy (XPS), and temperature-programmed desorption (TPD).

The Rh(111) crystal was prepared for this study as follows: the rough-cut crystal was first placed into a tube furnace where it was annealed at 1275 K in a 36-sccm flow of 99.999% H_2 for 4 days. For several years we have found this procedure to be very effective at removing boron and other light element contaminants from the crystal (*15*). Next, *both sides* of the Rh(111) single crystal were oriented to the (111) face within 1°, as shown by the Laue diffraction pattern. The sample was then sanded and polished with diamond paste with the final polish being 0.25 μ grit. Next, the sample was etched in hot (<375 K) 3 : 1 HCl : HNO_3. The sample was then mounted on the transfer device using etched 0.015″ Ta wires which were spot-welded to the edges of the crystal. Welding to the edges did not damage the polished faces and covered much of the non-(111) Rh on the crystal sides. The Rh(111) crystal was rectangular with an area of 52.3 mm^2 per side. The crystal was about 0.9 mm thick. A 0.003″ chromel–alumel thermocouple was spot-welded in the center of an edge of the crystal which did not contain a Ta heating lead.

A sharp (1 × 1) LEED pattern was obtained by Ar^+ sputtering (2 KeV, 20 μA) for 24 hr per side with the crystal at 875 K, followed by annealing in UHV at 1175 K for 2 hr. This extensive sputtering treatment was necessary to obtain a sharp LEED pattern. Next, the crystal was placed in the reactor and treated in 8 Torr CO/8 Torr O_2 at 525 K. This treatment was required to remove residual carbon from the near surface region of the sample. Surface cleanliness and order was checked with XPS and LEED, respectively.

After cleaning, the sample was drawn into the reactor and the gate valve to the UHV system closed. The reactor was of relatively small volume (652 ml) and was pumped with a turbo-molecular pump. Typical base pressures in the reactor were about 10^{-9} Torr before introduction of the reactants. For all of the rate measurements reported here, CO and N_2O were mixed in the reactor at low pressures. The N_2O (Matheson 99.0%) was trapped at 225 K using a liquid nitrogen and ethylene glycol slurry. The CO (Scott 99.99% in an Al cylinder) was trapped with a liquid-nitrogen bath which excluded any metal carbonyls from the reactor. The pressure in the reactor was measured using a baratron gauge.

Reactions were done in a batch mode and the products and reactants were measured with a GC using a 6′ × ⅛″ stainless steel HAYESEP N column operated at 323 K with a He carrier gas. Column effluents were monitored using both a flame ionization detector (FID) and a thermal conductivity detector (TCD) which were in series. Gases passed first through the TCD, then through a methanizer with a Ni catalyst, and then to the FID. Using this arrangement we were able to detect NO (TCD), CO (TCD and FID), N_2O (TCD), and CO_2 (TCD and FID). N_2 was detectable with the TCD; however, our column did not separate N_2 from CO, making quantification of the amount of N_2 unreliable. However, by comparison of the TCD (CO + N_2) and FID (CO only) signals we could qualitatively observe N_2 as a product. The experimental procedure for making a rate measurement was as follows: (1) the reactants were leaked into the reactor, (2) the sample was ramped to the reaction temperature (570 K $\leq T \leq$ 670 K) at 10 K/sec, (3) the timer was started when the sample was within 5° of the reaction temperature, (4) the temperature was held (±2°) for a specified time interval, (5) the sample was cooled to room temperature, and (6) after 5 min the gases in the reactor were expanded into an evacuated GC line. GC data were stored on our laboratory computer for analysis.

2.2 Sources of Errors

There are several sources of error which must be carefully avoided when performing batch reactions. One potential problem is poor mixing and/or diffusion within the reactor. We performed several experiments that assured us that the reactant gases were properly mixed and that the reaction was not diffusion-limited. For these experiments we used He as a diluent to vary the total pressure in the reactor while keeping the partial pressures of the reactants constant. In this case, the premixed reactants were leaked into the reactor, He was added to increase the total pressure, and the reaction was run for a fixed amount of time. Above 500 Torr total pressure, we found that GC signals for the products tended to change with time elapsed after the reaction, suggesting that the gases in the reactor were diffusion-limited. We avoided this condition by operating the reactor below 40 Torr at all times.

Another source for systematic error in the rate measurements is an inaccurate reading of the sample temperature during the reaction. Accuracy of the thermocouple measurement was checked in two ways. First, we immersed the sample in controlled temperature baths in the range of 273 to 373 K finding less than 1 K error in the thermocouple reading over this temperature range. For higher temperatures we attached a second thermocouple to the sample and compared its reading with that of the thermocouple used for these experiments. The sample was then heated by two methods, resistively (as during the rate measurements) and with a heat gun (to eliminate any potential ohmic drop across the sample). We found that these two thermocouple readings agreed within 2 K between 375 and 475 K. Based on these experiments we concluded that we were very accurately measuring the sample temperature during the course of these experiments.

A third potential source of error is reactive surfaces other than the Rh single crystal in the system. Our primary concern was that the Ta leads or the chromel–alumel thermocouple were catalytically active. To check this possibility we mounted a single Ta wire with a thermocouple attached to it in the system. The Ta wire was found to be catalytically inactive below 675 K; therefore, we can attribute all of the observed catalytic activity to the Rh(111) single crystal.

Another potential source of error in the rate measurements is product that is formed during the heating to and cooling from the reaction temperature. For reactions with relatively large activation energies the amount of product formed at lower temperatures is relatively small. Therefore, this ef-

fect leads to a relatively small uncertainty in the measured rate.

3. RESULTS

3.1. Experiment

When CO and N_2O were reacted over Rh(111) only CO_2 and N_2 were observed as products, in agreement with previous results (*4*). Figure 1 shows the CO_2 turnover number (TON) plotted versus $1/T$ for the reaction of 4 Torr CO and 4 Torr N_2O between 570 and 670 K. The dashed line shows a fit of the data with the model discussed below. Linear regression analysis of the data in Fig. 1 gives an apparent activation energy (E_a) for the reaction of 40.0 kcal/mol with an uncertainty of +2.6 and −3.1 kcal/mol. The uncertainty in E_a was estimated by determining a maximum and minimum slope (as defined by the error bars on the data points) for a line through the data in Fig. 1. The preexponential factor (ν) is estimated to be 7×10^{13} CO_2 site^{-1} sec^{-1}.

Figure 2 shows the CO_2 TON versus pressure of a given reactant with the second reactant held constant at 4 Torr. The reaction temperature was 623 K. A linear regresson analysis of the two data sets gives reaction orders of −1.18 in CO pressure and +1.14 order in N_2O pressure the uncertainty in both these results is ±0.15. The dashed lines are the model predictions which have reaction orders of −1.0 in CO and +1.0 in N_2O.

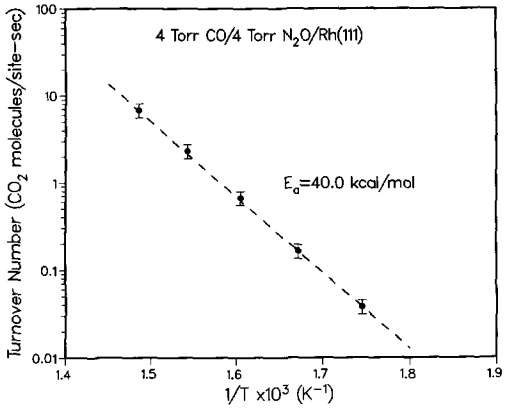

FIG. 1. Rate for the CO + N_2O reaction measured using $P^{CO} = P^{N_2O} = 4$ Torr (circles) and the rate predicted from the model (dashed line).

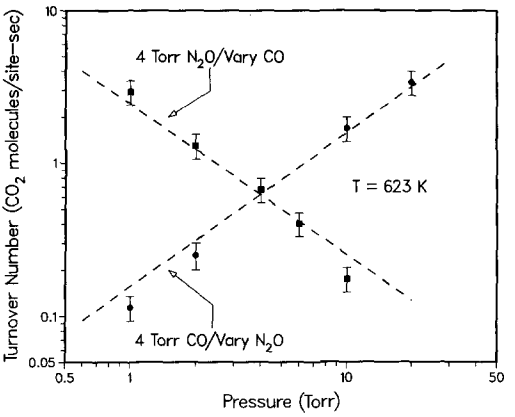

FIG. 2. Rate for the CO + N_2O reaction vs pressure of the individual reactants. The squares are for a fixed $P^{N_2O} = 4$ Torr with a varying P^{CO}. The circles are for fixed $P^{CO} = 4$ Torr with varying P^{N_2O}. The reactions were run at 623 K.

3.2. Model

In order to model the kinetic data shown in Figs. 1 and 2 we require: (1) a mechanism consisting of elementary reaction steps, (2) rate expressions for each reaction step, (3) rate constants for each step, and (4) a set of steady-state conservation equations for the surface species. With these four items in hand, we can calculate the overall reaction rate from the steady rate surface concentrations.

3.2.1. CO + N_2O mechanism. The kinetic data of Figs. 1 and 2 are modeled using a mechanism which consists of the elementary steps

$$CO_g + S \rightleftharpoons CO_a \quad (1)$$

$$N_2O_g + S \rightleftharpoons N_2O_a \quad (2)$$

$$N_2O_a \rightarrow N_{2g} + O_a \quad (3)$$

$$CO_a + O_a \rightarrow CO_{2g} + 2S, \quad (4)$$

where the subscript "a" refers to adsorbed

and "g" refers to gas phase. This is the same mechanism proposed by McCabe and Wong (*4*) for the reaction of CO and N_2O over supported Rh particles and is based on the widely accepted assumption that CO is oxidized via a surface reaction between CO_a and O_a (*3, 4, 6–8, 11, 12*). Surface O atoms are generated in step (3), when N_2O_a dissociates to gives O_a and N_{2g}. O_a and N_{2g} are the dissociation products that were observed for N_2O adsorbed on Rh(111) (*16*), Cu(111) (*17*), and Ni(110) (*18*). None of these groups reported the deposition of significant amounts of N_a from N_2O decomposition; therefore, N_a is not included in the mechanism. CO_{2g} is formed by reaction of O_a and CO_a in step (4). This reaction step has been successfully employed many times to explain CO oxidation by a variety of oxidants (*3, 4, 7, 8, 11, 12*). Step (4) has CO_2 forming on and desorbing from the surface in a single irreversible step based on the assumption that under these reaction conditions CO_2 desorption is much faster than CO_2 dissociation or formation.

3.2.2. Rate expressions. Once we propose a mechanism, our next requirement is a rate expression for each of the steps. We choose to use rate expressions which have been previously proposed to model the CO + N_2O (*4*) and CO + O_2 (*11*) reactions.

The rates for adsorption of CO (r_{ads}^{CO}) and N_2O ($r_{ads}^{N_2O}$) can be derived readily from the kinetic theory of gases (*19, 20*). For CO adsorption we obtain

$$r_{ads}^{CO} = F_{CO}\,\sigma\,S_{CO}\Theta_V,$$

where Θ_V ($0 \leq \Theta_V < 1$) is the fraction of sites which are vacant, F_{CO} is the flux of CO_g at the surface, σ is the area per mole of Rh(111) surface atoms (3.75×10^8 cm^2), and S_{CO} is the CO sticking coefficient. A similar expression describes the N_2O adsorption rate ($r_{ads}^{N_2O}$).

As for CO desorption, we assume that the desorption rate (r_{des}^{CO}) is first order in CO coverage (Θ_{CO}) and has an activation energy (E_{des}^{CO}) which is coverage dependent. Under these assumptions

$$r_{des}^{CO} = \nu \exp[-(E_{des}^{CO} - \alpha_{CO}\Theta_{CO})/RT]\Theta_{CO},$$

where ν is a coverage-independent preexponential factor and α_{CO} accounts for the dependence of E_{des}^{CO} on Θ_{CO}. Although this is certainly an over-simplification of CO desorption kinetics, this same expression was successfully used to model CO oxidation by oxygen (*11*) under conditions where CO is desorbing from a surface with a high CO coverage.

For N_2O desorption we use a first order rate expression and a coverage-independent activation energy. We neglect the small coverage dependence of E_a (0.5 kcal/mol) that Avery (*21*) used to describe N_2O desorption from Pt(111), because our calculations show that at steady state Θ_{N_2O} is less than 10^{-7} ML.

For the dissociation of absorbed N_2O, we assume the rate expression is of the form

$$r_{diss}^{N_2O} = \nu \exp[-E_a/RT]\Theta_{N_2O}.$$

Our assumption here is that a vacant site is not required in order for N_2O dissociation. In other words, the O atom is left in the same site that the N_2O_a molecule occupied.

The rate expression for the step that forms CO_2 is assumed to be of the form

$$r_{CO_2} = \nu \exp[-E_a/RT]\Theta_O\Theta_{CO}. \qquad (5)$$

3.2.3 Rate constants. After we establish the rate expression for each reaction step, we must choose a value for each of the rate parameters. Table 1 shows the values which were used in the model. Whenever possible, we have used values obtained by independent rate measurements for that particular elementary step. Unfortunately, little or no data exist for the adsorption, desorption, and decomposition of N_2O on Rh(111). For N_2O desorption, we used the parameters determined by Avery for desorption from Pt(111) (*21*). As for N_2O sticking, we have set S_{N_2O} to 0.5, roughly the value Daniel *et al.* (*16*) measured for dissociative sticking of N_2O on Rh(100). The rate parameters for N_2O dissociation were treated as adjustable

TABLE 1

Kinetic Parameters for the CO + N_2O Reaction

Reaction	Rate equation	Parameter	Value
1. $CO_g + S \rightarrow CO_a$	$F_{CO}\,\sigma\,S_{CO}\,\Theta_V$	S_{CO}	0.5[a]
2. $CO_a \rightarrow CO_g + S$	$\nu \exp\left[\frac{-(E-\alpha\Theta)}{RT}\right]\Theta_{CO}$	ν	1.0×10^{13} s^{-1}[b]
		E_{des}^{CO}	30.0 kcal/mol[b]
		α_{CO}	2.0 kcal/mol[b]
3. $N_2O_g + S \rightarrow N_2O_a$	$F_{N_2O}\sigma S_{N_2O}\,\Theta_V$	S_{N_2O}	0.5[c]
4. $N_2O_a \rightarrow N_2O_g + S$	$\nu \exp\left[\frac{-E}{RT}\right]\Theta_{N_2O}$	ν	1.0×10^{13} s^{-1}[d]
		$E_{des}^{N_2O}$	5.6 kcal/mol[d]
5. $N_2O_a \rightarrow N_{2g} + O_a$	$\nu \exp\left[\frac{-E}{RT}\right]\Theta_{N_2O}$	ν	6.5×10^{13} s^{-1}[e]
		$E_{diss}^{N_2O}$	17.5 kcal/mol[e]
6. $CO_a + O_a \rightarrow CO_{2g} + 2S$	$\nu \exp\left[\frac{-E}{RT}\right]\Theta_{CO}\Theta_O$	ν	1.0×10^{12} s^{-1}[f]
		$E_{form}^{CO_2}$	14.3[g]

[a] Same as literature values (*4, 11, 22*).
[b] From fits of our CO TPD data from Rh(111).
[c] Same as literature values (*4, 16*).
[d] Literature values for desorption from Pt(111) (*21*).
[e] Adjusted to fit the experimental data.
[f] Selected as a generic preexponential factor (*11*).
[g] Literature value (*11, 24*).

parameters, because we were unable to find measurements of the N_2O dissociation rate on Rh surfaces.

CO adsorption and desorption rates have been measured extensively on Rh(111). It is well established that initial CO sticking coefficient is quite high (*22*). Following Oh *et al.* (*11*) and McCabe and Wong (*4*), we choose S_{CO} as 0.5. For CO desorption, we use values that were obtained by fitting temperature-programmed desorption data from our Rh(111) crystal. CO desorbs from Rh in at least two overlapping peaks (*22, 23*); however, our model has only a single rate expression (or peak) for CO desorption. The parameters shown in Table 1 give a very good fit to the high-temperature CO desorption peak which fills first on Rh(111). In essence, we are assuming that CO desorption from the low-temperature TPD peak is not important under our reaction conditions. The CO desorption parameters in Table 1 give desorption rates at 625 K that are about 30× slower than the values used previously by Oh *et al.* (*11*) to model CO + O_2 and those of McCabe and Wong (*4*) to model CO + N_2O. We chose to re-evaluate the CO desorption parameters upon finding that those used previously (*4, 11*) could not adequately describe the data that we obtained, especially that of Fig. 2. This point is discussed further in Section 4.2.

For the CO_2 formation step, we use the same rate constants as employed by Oh *et al.* (*11*). Following Oh *et al.*, we use the same barrier, E_a = 14.3 kcal/mol, as was measured by Campbell *et al.* (*24*) for CO + O over polycrystalline Rh; however, we use a preexponential, 10^{12} sec^{-1}, more indicative of a second-order surface reaction. We note that the overall reaction rate is quite insensitive to this rate constant, because N_2O dissociation is the RLS (see Section 4.4).

3.2.4. Steady-state equations. Our mechanism includes three adsorbates, CO_a, O_a, and N_2O_a. The steady-sate conservation equations for these species are

$$r_{ads}^{CO} - r_{des}^{CO} - r_{form}^{CO_2} = 0, \quad (6)$$

$$r_{ads}^{N_2O} - r_{des}^{N_2O} - r_{diss}^{N_2O} = 0, \quad (7)$$

$$r_{diss}^{N_2O} - r_{form}^{CO_2} = 0. \quad (8)$$

The calculate the overall reaction rate we specify the reaction conditions (P^{N_2O}, P^{CO},

T), solve Eqs. (6)–(8) for the steady-state adsorbate coverages, and then calculate the TON from Eq. (5).

4. DISCUSSION

4.1. Comparison to Supported Rh

The reason that we studied the CO + N_2O reaction over a Rh(111) catalyst is to gain a better understanding of this reaction over conventional supported catalysts. In order to establish this connection, we must compare the Rh(111) kinetics to those observed for supported Rh. McCabe and Wong have previously studied the CO + N_2O reaction over alumina-supported Rh (*4*). We chose our reaction temperatures and pressures to make for easy comparison to their experiments. McCabe and Wong do not report TONs for their supported catalyst, but by most other measures the kinetics for Rh(111) are, within experimental error, identical to those for supported Rh. For instance, McCabe and Wong (*4*) reported that E_a for the reaction is 40.5 kcal/mol; we measure 40.0 kcal/mol (Fig. 1). They reported reaction orders in CO pressure of -1.1 at 564 K and -0.86 at 583 K. The model which fits our data at 625 K (Fig. 2) has a reaction order of -1.0. The only area of significant difference between Rh(111) and supported Rh appears to be in the N_2O pressure dependence. Whereas McCabe and Wong (*4*) reported a reaction order (P^{N_2O}) of $+0.65$, we measure $+1.1$. They speculated that the fractional order reflected a complicated precursor adsorption kinetics as opposed to simple single site adsorption. The data that we obtain is somewhat easier to rationalize for a CO oxidation reaction on a surface with a very high CO coverage (*4, 11, 12*). Overall, we conclude that Rh(111) is a good model for a supported Rh particle with regards to the CO + N_2O reaction.

4.2. Kinetic Modeling

All of the experimental data that we obtained were quite adequately modeled using the mechanism described in Section 3.2. To reiterate, we relied heavily on experimentally determined rate constants; however, we fit the data by adjusting $k_{diss}^{N_2O}$. In our model both CO and N_2O have equal probabilities of sticking on an open site. Although this is almost certainly incorrect, it does provide for a good framework within which we can examine the remaining rate constants in the system. Below we discuss the possible values of S_{N_2O} in more detail.

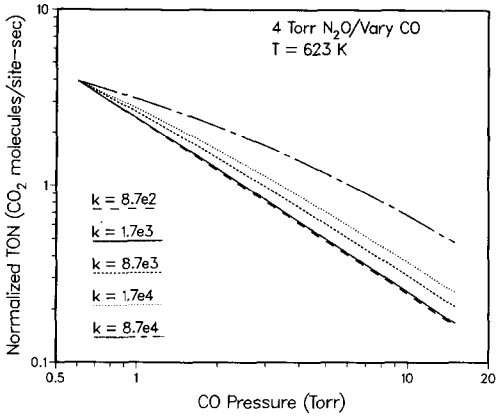

FIG. 3. Rates calculated from the model using different rate constants, k_{des}^{CO}, for the CO desorption step. Calculations are for varying P^{CO} with P^{N_2O} = 4 Torr and T = 623 K. Experimental data were modeled (see Fig. 2) with $k_{des}^{CO} = 1.7 \times 10^3$ (solid line).

The overall reaction rate is controlled by three rate constants, k_{des}^{CO}, $k_{diss}^{N_2O}$, and $k_{des}^{N_2O}$. The first one, k_{des}^{CO}, sets the CO desorption rate which controls the number of open sites available for reaction. CO desorption controls the reaction rate because O_a and N_2O_a are removed from the surface very rapidly through reaction (step 4) and desorption (reverse of step 2), respectively. For instance, when $P^{CO} = P^{N_2O} = 4$ Torr and $T = 625$ K, then $\Theta_{CO} \approx 0.995$ ML and $\Theta_V \approx 0.005$ ML ($\Theta_{N_2O} \approx \Theta_O \leq 10^{-7}$ ML). In situations where CO, which is strongly adsorbed, competes with a weakly adsorbed oxidant (N_2O) for the limited number of vacant sites, the reaction is typically negative first order in the CO and positive first order in the oxidant (N_2O).

Interestingly, our model predicts that the CO reaction order is very sensitive to the CO desorption rate. Figure 3 shows the pre-

dicted TON versus P^{CO} for different values of k_{des}^{CO} at 625 K. The reaction rates are normalized at $P^{CO} = 0.6$ Torr in order to isolate the effect of k_{des}^{CO} on the reaction order. In Fig. 3 the solid line has negative first-order kinetics and is obtained from the parameters in Table 1 which gave a good fit to our experimental data. We find that the experimentally observed negative first-order kinetics are predicted only when $k_{des}^{CO} \approx 2 \times 10^3$ sec^{-1} or less. For higher desorption rates Θ_{CO} drops below about 0.9 ML ($P^{CO} = 0.6$ Torr, $T = 625$ K) and the model predicts a fractional-order P^{CO} dependence. It is interesting to note that the value for k_{des}^{CO} ($\approx 2 \times 10^3$ s^{-1}) required to explain our CO + N_2O reaction kinetics is very close to that ($k_{des}^{CO} = 1.7 \times 10^3$ s^{-1}) which describes CO desorption rates in the *low coverage* limit when only the high-temperature CO TPD state is populated (*22*). This similarity in k_{des}^{CO} suggests that the CO + N_2O reaction kinetics are controlled by desorption out of this high-temperature CO TPD state. Previously, the CO + O_2 reaction kinetics were modeled very well (*11*) with $k_{des}^{CO} \approx 6 \times 10^4$ sec^{-1} over temperatures (600 K $\geq T \geq$ 450 K) somewhat lower than those examined here. For that case (*11*), k_{des}^{CO} is very close to the value ($\approx 8 \times 10^4$ sec^{-1}) we estimate (from fits of our CO TPD data) for desorption from the low-temperature CO TPD state. These similarities in k_{des}^{CO} suggest that CO desorption from the low-temperture CO TPD state plays a more important role in the CO + O_2 reaction than for the CO + N_2O reaction. We speculate that bridging CO, which is usually associated with the low temperature TPD state, is more important in inhibiting O_2 dissociation and thus controls the CO + O_2 reaction rate. This would be the case if O_2 dissociation occurs at these bridging sites. However, for the CO + N_2O reaction we speculate that linear or high desorption temperature CO inhibits the adsorption and/or dissociation of N_2O. Hence, two different CO desorption rates are necessary to adequately model both reactions.

In addition to k_{des}^{CO}, the reaction rate is also very sensitive to the ratio, $k_{diss}^{N_2O}/k_{des}^{N_2O}$, which is the probability that N_2O_a will dissociate. For $k_{des}^{N_2O}$ we used the values reported by Avery for Pt(111) (*21*). We were unable to obtain N_2O TPD spectra because we can only cool our sample to about 130 K—N_2O desorbs around 100 K. Then, we adjusted $k_{diss}^{N_2O}$ in order to fit our experimental data which leads to $k_{diss}^{N_2O}/k_{des}^{N_2O} = 5 \times 10^{-4}$. The value of $k_{diss}^{N_2O}$ which fits our experimental data depends linearly on the values for CO desorption rate and S_{N_2O} that we chose. As noted above, an upper limit on k_{des}^{CO} is established by the reaction order data which requires that CO coverage remain above 0.9 ML. With regards to N_2O sticking, if we had selected a lower value for S_{N_2O} then a proportionally larger value for $k_{diss}^{N_2O}$ would have been required to model the data (see Section 4.4).

4.3. Apparent Activation Energy

The model (Fig. 1, dashed line) is in good agreement with the experimentally determined E_a of 40.0 kcal/mole (Fig. 1, circles). The model's prediction for E_a is very closely approximated by

$$E_a = E_{des}^{CO} + E_{diss}^{N_2O} - E_{des}^{N_2O}. \qquad (9)$$

For the parameters in Table 1, Eq. (9) equals 39.9 kcal/mol when $\Theta_{CO} \approx 1$. Most importantly, the relationship in Eq. (9) allows us to establish, within a couple of kcals, the barrier for N_2O dissociation. This follows since E_{des}^{CO} and $E_{des}^{N_2O}$ are fairly well established. For Rh(111), E_{des}^{CO} is known to be 29.5 $\pm$ 2.5 kcal/mol (*4, 11, 22*). Further, given the very low N_2O desorption temperature $E_{des}^{N_2O}$ must be 5.6 $\pm$ 1.0 kcal/mol, the value measured for Pt(111) (*21*). Taking these values for E_{des}^{CO} and $E_{des}^{N_2O}$, $E_{diss}^{N_2O}$ is estimated to be 17.5 $\pm$ 3.5 kcal/mol. This prediction is helpful since $E_{diss}^{N_2O}$ has not been previously measured experimentally. Further, with $E_{diss}^{N_2O}$ fixed we can establish that N_2O dissociation is the RLS.

4.4. Rate-Limiting Step

The model predicts that the RLS is the dissociation of adsorbed N_2O. This is a di-

rect result of our choice of a high N_2O sticking coefficient. Under the assumption that S_{N_2O} is high and at $\Theta_{CO} \geq 0.9$ ML, the overall reaction rate is controlled by the ratio $k_{des}^{N_2O}/k_{diss}^{N_2O}$. With $S_{N_2O} = 0.5$, then $k_{des}^{N_2O}/k_{diss}^{N_2O}$ is about 2000 at 625 K so that N_2O dissociation limits the overall reaction rate. However, we must consider the possibility that N_2O adsorption is slow (S_{N_2O} is small) which could make N_2O adsorption rate limiting. Our model predicts that this is not the case. We estimate a lower limit for S_{N_2O} of 0.005 by estimating the maximum $r_{diss}^{N_2O}$ as follows: In Section 4.3 we established that $E_{diss}^{N_2O}$ must be 17.5 ± 3.5 kcal/mol in order to have E_a be 40.0 kcal/mol. Assuming that the preexponential factor for step (3) is $\leq 5 \times 10^{14}$, which is generally true for surface reactions, and that $E_{diss}^{N_2O} = 14.0$ kcal/mol (which maximizes $r_{diss}^{N_2O}$), then S_{N_2O} must be 0.005 in order to explain the experimental data (Figs. 1 and 2) With these rate constants, $r_{diss}^{N_2O}$ is roughly 20× slower than $r_{ads}^{N_2O} \approx r_{des}^{N_2O}$; therefore, N_2O dissociation is still the RLS. Furthermore, this analysis sets limits for S_{N_2O} ($1 \geq S_{N_2O} \geq 0.005$), a quantity for which no independent measurements exist.

5. CONCLUSIONS

We have, for the first time, measured the oxidation of CO by N_2O over Rh(111) and can quite accurately describe the observed kinetics with a model based on elementary reaction steps. Our experimental results show that the reaction is negative first order in CO pressure and positive first order in N_2O pressure with an apparent activation energy of 40.0 kcal/mol. Our modeling suggests that the reaction takes place on a surface with a CO coverage greater than 0.9 ML. Also, we conclude that the RLS for the reaction is the dissociation of adsorbed N_2O, this step has a barrier of roughly 17.5 kcal/mol. As for the adsorption of N_2O, we conclude that S_{N_2O} must be greater than 0.005 in order to adequately explain the kinetics that we observe. Our experimental data shows that Rh(111) is a very good model for a supported Rh catalyst for the CO + N_2O reaction, and our modeling establishes the RLS and allows us to estimate two previously unknown quantities, S_{N_2O} and $E_{diss}^{N_2O}$.

ACKNOWLEDGMENTS

The authors gratefully acknowledge our many helpful discussions with Se Oh and Galen Fisher of General Motors Research Laboratories.

REFERENCES

1. Taylor, K. C., *CHEMTECH* **20,** 551 (1990).
2. Taylor, K. C., "Automobile Catalytic Converters." Springer-Verlag, Berlin, 1984.
3. Cho, B. K., Shanks, B. H., and Bailey, J. E., *J. Catal.* **115,** 486 (1989).
4. McCabe, R. W., and Wong, C., *J. Catal.* **121,** 422 (1990).
5. Cho, B. K., and Shanks, B. H., Presented at the 1986 annual meeting of the to American Institute of Chemical Engineers, Miami Beach, FL.
6. Oh, S. H., *J. Catal.* **124,** 477 (1990).
7. Hecker, W. C., and Bell, A. T., *J. Catal.* **84,** 200 (1983).
8. Hecker, W. C., and Bell, A. T., *J. Catal.* **85,** 389 (1984).
9. Chin, A. A., and Bell, A. T., *J. Phys. Chem.* **87,** 3700 (1983).
10. Iizuka, T., and Lunsford, J. H., *J. Mol. Catal.* **8,** 39 (1980).
11. Oh, S. H., Fisher, G. B., Carpenter, J. E., and Goodman, D. W., *J. Catal.* **100,** 360 (1986).
12. Peden, C. H. F., Goodman, D. W., Blair, D. S., Fisher, G. B., Berlowitz, P. J., and Oh, S. H., *J. Phys. Chem.* **92,** 1563 (1988).
13. Hendershot, R. E., and Hansen, R. S., *J. Catal.* **98,** 150 (1986).
14. Belton, D. N., and Schmieg, S. J., in preparation.
15. Fisher, G. B., and Schmieg, S. J., *J. Vac. Sci. Technol. A* 1:1064, 1983.
16. Daniel, W. M., Kim, Y., Peebles, H. C., and White, J. M., *Surf. Sci.* **111,** 349 (1982).
17. Habraken, F. H. P. M., Kieffer, E. Ph., and Bootsma, G. A., *Surf. Sci.* **83,** 45 (1979).
18. Hoffman, D. A., and Hudson, J. B., *Surf. Sci.***180,** 77 (1987).
19. Somorjai, G. A., "Principles of Surface Chemistry." Prentice-Hall, Englewood Cliffs, NJ, 1972.
20. Herz, R. K., and Marin, S. P., *Surf. Sci.* **65,** 281 (1980).
21. Avery, N. R., *Surf. Sci.* **131,** 501 (1983).
22. Thiel, P. A., Williams, E. D., Jr., Yates, J. T., and Weinberg, W. H., *Surf. Sci.* **84,** 54 (1979).
23. Root, T. W., Schmidt, L. D., and Fisher, G. B., *Surf. Sci.* **150,** 173 (1985).
24. Campbell, C. T., Shi, S.-K., and White, J. M., *Surf. Sci.* **2,** 382 (1979).